

# Image-Guided Autonomous Guidewire Navigation in Robot-Assisted Endovascular Interventions using Reinforcement Learning

Wentao Liu<sup>1</sup>, Tong Tian<sup>2</sup>, Weijin Xu<sup>1</sup>, Bowen Liang<sup>3</sup>, Qingsheng Lu<sup>3</sup>, Xipeng Pan<sup>4</sup>, Wenyi Zhao<sup>1</sup>, Huihua Yang<sup>1,4</sup>(✉), and Ruisheng Su<sup>5</sup>

<sup>1</sup> School of Artificial Intelligence, Beijing University of Posts and Telecommunications, Beijing, China  
liuwentao@bupt.edu.cn

<sup>2</sup> Laboratory of Structural Analysis, Optimization and CAE Software for Industrial Equipment, School of Aeronautics and Astronautics, Dalian University of Technology, Dalian University of Technology, Dalian, China

<sup>3</sup> Department of Vascular Surgery, Shanghai Changhai Hospital, Naval Medical University, Shanghai, China

<sup>4</sup> School of Computer Science and Information Security, Guilin University of Electronic Technology, Guilin 541004, China

<sup>5</sup> Department of Radiology & Nuclear Medicine, Erasmus MC, University Medical Center Rotterdam, The Netherlands

**Abstract.** Autonomous robots in endovascular interventions possess the potential to navigate guidewires with safety and reliability, while reducing human error and shortening surgical time. However, current methods of guidewire navigation based on Reinforcement Learning (RL) depend on manual demonstration data or magnetic guidance. In this work, we propose an Image-guided Autonomous Guidewire Navigation (IAGN) method. Specifically, we introduce BDA-star, a path planning algorithm with boundary distance constraints, for the trajectory planning of guidewire navigation. We established an IAGN-RL environment where the observations are real-time guidewire feeding images highlighting the position of the guidewire tip and the planned path. We proposed a reward function based on the distances from both the guidewire tip to the planned path and the target to evaluate the agent's actions. Furthermore, in policy network, we employ a pre-trained convolutional neural network to extract features, mitigating stability issues and slow convergence rates associated with direct learning from raw pixels. Experiments conducted on the aortic simulation IAGN platform demonstrated that the proposed method, targeting the left subclavian artery and the brachiocephalic artery, achieved a 100% guidewire navigation success rate, along with reduced movement and retraction distances and trajectories tend to the center of the vessels.

**Keywords:** Endovascular interventions · Autonomous guidewire navigation · Image-guided · Reinforcement learning.

## 1 Introduction

Cardiovascular diseases continue to be the leading cause of mortality worldwide [18]. Endovascular Intervention (EI) represents a sophisticated technique in the realm of endovascular therapy, primarily employed for the diagnosis and treatment of cardiovascular diseases. Characterized by minimal invasiveness, rapid recovery, and low complication rates, EI is extensively applied in the management of various cardiovascular conditions, such as aortic disease, peripheral arterial disease, and stroke. Despite its advantages, EI still presents some drawbacks such as lack of sensory feedback, surgeon exposure to radiation, and the need for highly dexterous manipulation. In response to the ongoing radiation exposure risk faced by surgeons during fluoroscopic procedures, a variety of robotic systems employing leader-follower teleoperation architecture have been introduced. However, compared to the direct manipulation of surgical instruments like guidewires and catheters, the learning curve for operating surgical robots is substantially increased [1]. Additionally, current EI robots lack autonomy, indicating a significant reliance on direct physician control and guidance. A highly autonomous surgery would ideally inflict little damage whilst operating in a timely manner [7].

Recently, the autonomous functions of EI robots have been progressively refined, giving rise to several outstanding developments. Such systems leverage deep learning such as Convolutional Neural Network (CNN) and generative adversarial networks to facilitate surgical status prediction [19], catheter tip tracking [15], vessel segmentation [13,17], and automate catheterization [1]. Moreover, deep Reinforcement Learning (RL) techniques have the capability to model extensive, continuous state spaces, thus facilitating the automation of intricate EI tasks. It can learn relevant behavioral patterns from human demonstrations, which encapsulate surgical operational experience, by updating strategies through interaction with the environment [2,1,11]. Currently, autonomous guidewire navigation has been successfully implemented in virtual surgical environments [8] and on two-dimensional planar vascular platforms [11,10]. However, dependence on manual demonstrations limits the scalability of these methods, and electromagnetic-based guidewire positioning proves impractical for real-world surgical scenarios [5].

In this paper, we propose an Image-guided Autonomous Guidewire Navigation (IAGN) method for EI that operates independently of human demonstrations. As shown in the Fig. 1, firstly, we utilize FR-UNet [14] and YOLOv8 [9] to facilitate the segmentation of vascular models and the localization of the guidewire tip within the images captured by IAGN platform. We introduce the BDA-Star path planning algorithm, which simultaneously considers trajectory distance and boundary proximity. We also established an RL environment for guidewire navigation, which encompasses observations that integrate multi-image information and a reward function designed for path navigation. Furthermore, we have employed a pre-trained model for representation extraction, leveraging its prior knowledge in recognizing generic patterns and features within images. Experiments carried out on the aortic simulation IAGN platform have

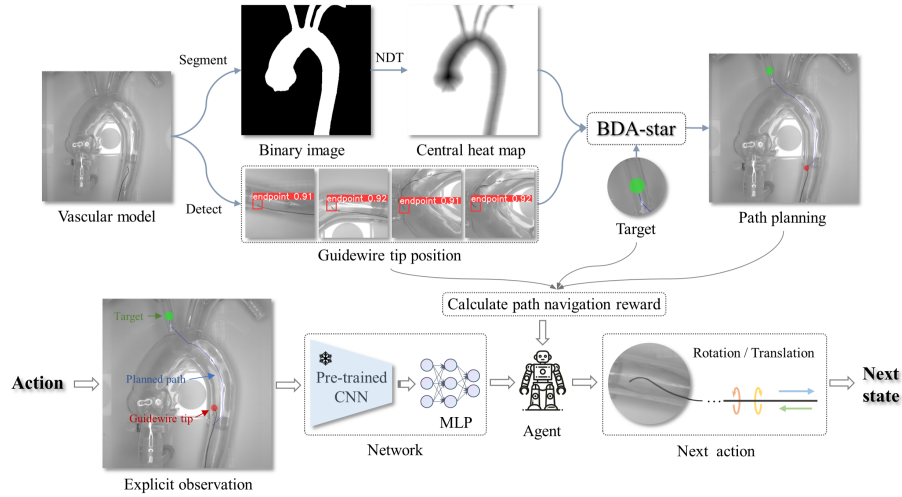


**Fig. 1.** Overview of the proposed image-guided autonomous navigation framework for endovascular interventions (NDT: Normalized Distance Transform).

shown that the proposed method, which targets the Left Subclavian Artery (LSA) and the Brachiocephalic Artery (BCA), achieved a 100% guidewire navigation success rate. Furthermore, this approach has led to reductions in both movement and retraction distances, with trajectories that consistently converge towards the central axis of the vessels.

## 2 Materials and Methods

### 2.1 Autonomous Guidewire Navigation Platform

As shown in the Fig. 2, we have established an IAGN platform comprised of a machine vision system, an anthropomorphic vessel model, a guidewire feeding robot, and compute server. The model comprises the femoral artery, iliac artery, Type-I aortic arch, and the carotid arteries, and is constructed from a silicone-based, transparent material. The guidewire employed for the task is a 0.035-inch nitinol guidewire, known for its exceptional flexibility and maneuverability. The machine vision system, consisting of a camera, lens, ring light, and a mount is vertically positioned right above the aortic arch to meet the requirements of guidewire navigation tasks. The captured images encompass the vasculature starting from the thoracic aorta and extending to either LSA or BCA. The right side of Fig. 2 presents our custom-designed guidewire feeding robot, which is capable of executing push-pull and rotational actions on the guidewire for conducting IAGN training through RL.

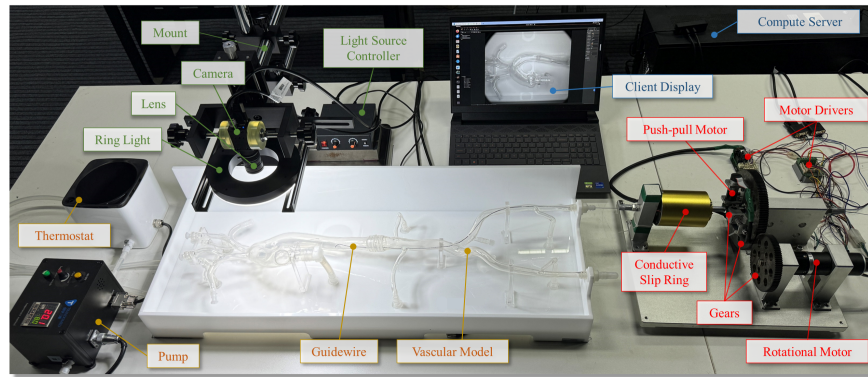


Fig. 2. Image-guided autonomous guidewire navigation platform.

## 2.2 Trajectory Navigation

The path planning of the guidewire and the accurate positioning of its tip are fundamental to achieving effective trajectory navigation during guidewire feeding. The following sections introduce the methods proposed for addressing them.

**Path Planning** In the guidewire navigation task, path planning is defined as determining the optimal path within the vessel between the guidewire tip and the target point (vessel branch or lesion). The most prevalent path planning algorithms are A-star [3] and its derivatives, which are based on heuristic pathfinding and graph traversal techniques. However, to apply these algorithms to EI, it is first necessary to segment the vessels to define their boundaries and thus confine the search space within the vessels. We collected 10 images of the vessel model and performed pixel-level annotations. These images were then used to train the 2D segmentation network, FR-UNet [14], specifically for vessel segmentation. The trained model is subsequently employed for the real-time segmentation of vascular models captured by the camera.

To minimize the path distance while directing the trajectory towards the center of the vessel and to reduce the likelihood of collisions between the guidewire tip and the vessel walls as much as possible, we propose BDA-star. This algorithm incorporates a boundary distance measure for each node into the cost function, enabling a balance between the costs of path length and boundary proximity. Specifically, we utilize the segmented vascular image to generate a boundary distance heatmap. Initially, a distance transformation is conducted on the segmented map to produce a heatmap representing the distance from each vascular pixel to the nearest zero pixel. Subsequently, a convolution kernel created based on the heatmap’s maximum value is used to convolve the segmented map. Finally, the heatmap is normalized by dividing it with the convolved image.

Let  $\mathbf{I}$  be the segmented map, the normalized heatmap  $\mathbf{H}$  is given by:

$$\mathbf{H} = \frac{D(\mathbf{I})}{\mathbf{I} * K_{\max(D(\mathbf{I}))}}, \quad (1)$$

where  $D(\mathbf{I})$  is the euclidean distance transform of  $V$ ,  $*$  represents the convolution operation, and  $K_{\max(D(\mathbf{I}))}$  is the convolution kernel generated from the maximum value of  $D(\mathbf{I})$ .

We define each pixel within the segmentation image as a node, represented by  $n$ . Among the paths expanded from each node, the path in the BDA-star algorithm is selected by minimizing the cost function:

$$f(n) = \underbrace{g(n) + h(n)}_{A\text{-star}} + \omega \mathbf{H}(n), \quad (2)$$

where  $g(n)$  is the cost of the path from the start node to node  $n$ ,  $h(n)$  is a heuristic function that estimates the cost from node  $g(n)$  to the goal. In IAGN task, the heuristic function is the Euclidean distance.  $\mathbf{H}(n)$  represents the distance between the node  $n$  and the nearest boundary node.  $W$  represents the weight of the boundary distance term. The greater the value of  $W$  is, the more closely the path aligns with the center of the vessel.

**Guidewire Tip Localization** Currently, the prevalent methods for locating the tip of guidewires primarily rely on image segmentation [20,6], with a minority employing a two-phase strategy that combines initial segmentation followed by detection [12]. To maximize the efficiency of localization, we directly employ object detection for the positioning of the guidewire tip. For this purpose, we recorded a 10-minute video of manual guidewire feeding, annotating these images with rectangular bounding boxes centered around the guidewire tip. Subsequently, we train this dataset using the one-stage detection framework YOLOv8 [9], resulting in a highly effective model that is utilized for real-time positioning of the guidewire tip during autonomous guidewire navigation.

### 2.3 Reinforcement Learning for Autonomous Guidewire Navigation

**Problem Definition** We conceptualize IAGN as an episodic partially observable markov decision process. The agent, embodied by the guidewire, navigates through an environment  $E$ , represented by the vessel model. At each discrete time step  $t$ , the agent receives an observation  $s_t$ , based on which it selects an action  $a_t(s_t)$ . This action leads to a reward  $r_t(s_t, a_t)$  and transitions the agent to a new state  $s_{t+1}$ . The episodic process culminates when the agent attains its goal position within the vessel, denoted as  $g$  in the goal state set  $G$ .

**Explicit Observations** In the IAGN platform, the camera deployed above the aorta captures real-time guidewire feeding images, akin to 2D Digital Subtraction

Angiography (DSA) seen in actual surgical scenarios [13]. The surgeon observes and analyzes these images to perform EI procedures. Likewise, in IAGN task, we consider only the guidewire feeding images as the observations for the agent. Specifically, we fuse the pre-planned path, target, and the real-time positioning of the guidewire tip with live imaging. This explicit observation capability is designed to focus the learning interest of RL task. This enhanced observation explicitly articulates useful state information, which aids in accelerating policy learning and improving the robustness of the algorithm.

**Actions** The actions are represented by a vector  $a_t \in \mathbb{R}^2$ , which are associated respectively with the push-pull motor that drives the guidewire’s translational movement and the motor responsible for the guidewire’s rotation. We have set the maximum translational distance  $S$  and the maximum rotation angle  $R$  for each action step of the guidewire, thereby establishing the action spaces as  $[-S, S]$  for translation and  $[-R, R]$  for rotation, respectively.

**Path Navigation Reward Function** In the context of an IAGN system, the reward function is designed to aid the system in guiding the guidewire tip towards a target point, typically within the vascular network of a patient during a medical procedure such as angiography or stent placement. The reward function is composed of two parts, reflecting different stages and strategies within the navigation process. (1) **Success Reward:** This is a fixed reward  $R_{success}$  given when the guidewire tip is within a threshold distance  $\delta$  from the target point. This condition reflects the successful completion of the navigation task. (2) **Continuous Reward:** When the guidewire tip is not within the threshold distance, the reward function is designed to encourage progress towards the target point and adherence to a pre-planned path, while penalizing deviations from the optimal trajectory and promoting smoothness of the trajectory. The formula for the reward function  $r(t)$  at time  $t$  is defined as:

$$r(t) = \begin{cases} R_{success}, & \text{if } \|x_t - g\|_2 \leq \delta \\ - \left( e^{\omega_1 \min_{k=1}^N \|x_t - p_k\|_2} + \omega_2 \sum_{k=j}^{N-1} \|p_{k+1} - p_k\|_2 \right), & \text{otherwise} \end{cases} \quad (3)$$

where  $x_t$  denotes the position of the guidewire tip at time  $t$ ,  $g$  represents the target point’s position. The norm  $\|\cdot\|_2$  denotes the euclidean distance.  $\omega_1$  and  $\omega_2$  are weighting factors that adjust the importance of the two terms in the continuous reward.  $N$  is the number of points on the planned path.  $p_k$  represents the  $k$ -th point on the planned path. The 1-st and  $N$ -th points serve as the starting and ending points, respectively.  $j$  is the index of the point on the pre-planned path that is closest to the guidewire tip, i.e.,  $\arg \min_{k=1, \dots, N} \|x_t - p_k\|_2$ .

**Network Architectures** We employ a pre-trained CNN to extract features from input images i.e., observations. During training, the weights of this CNN

model are frozen, and the resulting feature vectors are fed into a Multi-Layer Perceptron (MLP) for policy training. This approach leverages the pre-trained model’s prior knowledge in recognizing generic patterns and features within images. It offers a more stable and meaningful input space while effectively reducing data dimensionality.

### 3 Experiments

#### 3.1 Implementation Details

We employed the Soft Actor-Critic (SAC) algorithm for RL training in autonomous guidewire navigation. The experiments were conducted using PyTorch, and for the implementation of the SAC, we employed stable baselines [16]. We targeted the BCA and the LSA for guidewire navigation, with training time steps of 150,000 and 300,000, respectively. The maximum number of steps allowed for each episode was set to 50. The maximum values for actions  $S$  and  $R$  are set to 20 mm and  $90^\circ$ . We utilize a pre-trained ResNet50 [4] for feature extraction. In the reward function, the reward  $R_{success}$  for successful navigation is set to 50, and the threshold distance  $\delta$  is set to 40. The parameters  $\omega_1$  and  $\omega_2$  are set to 0.005 and 0.01, respectively. In DBA-star, the weight of the boundary distance term is set to 2. We conducted 20 tests each for the LSA and BCA tasks, calculating the Success Rates (ST), Rewards and Lengths of Episodes (ER, EL), Movement Distances (MD), Boundary Distances (BD), and Retracement Distances (RD) to evaluate the performance of the IAGN algorithm. We set a baseline using original images as observations, with the reward function’s second term being the negative euclidean distance between the target point and the guidewire tip’s real-time position [7], employing stable baselines’s CnnPolicy as the policy network. On the baseline, Pre-trained CNNs ( $PC$ ), Path Navigation Rewards ( $PNR$ ), and Explicit Observations ( $EO$ ) were incrementally integrated to evaluate the performance of each part as well as their collective efficacy.

#### 3.2 Results

As illustrated in Table 1, aside from the *baseline*, all methods achieved autonomous guidewire navigation within the target areas of LSA and BCA with a 100% success rate in fewer than maximum steps. This success is chiefly attributed to the strategy of employing the powerful  $PC$  for feature extraction.  $EO$  and  $PNR$  can be considered as the explicit and implicit guidance for IAGN agents in path navigation. Based on the  $PC$ ,  $EO$  and  $PNR$  both exhibit improvements across ER, EL, MD, and RD. Notably,  $EO$  achieves the highest EL and MD in the LSA task, reaching the target with the fewest steps and shortest movement distance. Furthermore,  $EO$  has significantly improved BD, indicating that integrating pre-planned path and guidewire tip information into observations is beneficial for policy learning that tends towards the center of vessels. The integration of  $PC$ ,  $EO$ , and  $PNR$  forms the core of the IAGN algorithm,

**Table 1.** Experiment results. † indicated that the continuous reward uses negative Euclidean distance, resulting in higher values than PNR. ‡ means the policy of *baseline* is restricted to forward motion and is not considered in the comparative evaluation.

Tasks	Methods			Metrics					
	<i>PC</i>	<i>EO</i>	<i>PNR</i>	SR % ↑	ER ↑	EL ↓	MD(mm) ↓	BD(px) ↑	RD(mm) ↓
LSA				65	-125.3±120.2 <sup>†</sup>	23.9±8.2	190.8±65.8	46.4±33.8	0 <sup>‡</sup>
	✓			100	9.8±6.9 <sup>†</sup>	13.0±3.8	182.2±43.9	44.5±29.1	24.7±22.1
	✓	✓		100	<b>17.7 3.2<sup>†</sup></b>	<b>8.2±1.5</b>	<b>141.6±12.9</b>	56.7±28.1	3.5±6.77
	✓		✓	100	6.9±4.8	10.1±3.0	148.7±15.3	46.0±32.8	5.9±6.5
	✓	✓	✓	100	<b>7.4 5.5</b>	<b>8.2±1.90</b>	143.2±11.2	<b>59.5±28.2</b>	<b>2.6±5.6</b>
BCA				15	-122.3±87.7 <sup>†</sup>	14.3±2.1	271.7.2±40.3	47.6±30.6	0 <sup>‡</sup>
	✓			100	-3.4±12.0 <sup>†</sup>	14.6±5.9	245.2±72.6	49.8±24.7	29.4±36.3
	✓	✓		100	<b>4.77±2.59<sup>†</sup></b>	12.3±2.1	226.0±52.4	53.5±29.4	13.5±14.1
	✓		✓	100	-14.3±14.1	13.3±4.2	228.6±59.5	46.1±23.7	23.0±26.6
	✓	✓	✓	100	<b>-8.3±8.3</b>	<b>10.4±0.8</b>	<b>184.5±4.9</b>	<b>62.3±25.8</b>	<b>0.1±0.4</b>

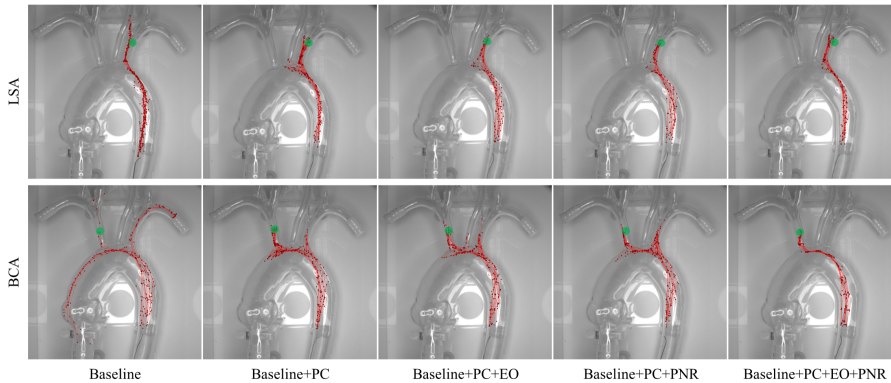


**Fig. 3.** Visualization of the path for autonomous guidewire navigation.

achieving the highest scores across numerous metrics. Specifically, in the more challenging BCA task, compared to the *baseline+PC*, there was a reduction of 28.7% in the average number of steps, a decrease of 24.8% in the movement, and an increase of 25.1% in the distance from the vascular boundary. Remarkably, the average distance for guidewire retraction was only 0.1mm.

We visualized the guidewire movement trajectories during testing, as shown in Fig. 3. The performance of *baseline* was poor, particularly in the BCA tasks, where most experiments resulted in the guidewire entering the LSA and ascending aorta, with the guidewire continuously moving forward without any action for retraction. This is consistent with the *baseline*'s RD being 0, as listed in Table 1, hence contributing to the lower success rate of guidewire navigation. The *baseline+PC* employs a pre-trained CNN to extract features and utilizes an MLP as the policy network. When the guidewire deviates from the planned path, the agent performs a retraction action. This is demonstrated in the LSA tasks, where the guidewire tip misses the LSA entrance and then returns, and



in the BAC tasks, where the guidewire tip enters the LSA and then retracts back to the aortic arch. From the Fig. 3, it is evident that the path point distributions for *baseline+PC+OB* and *baseline+PC+PNR* are similar. Importantly, the combination of all components achieved the best results. The path points for *baseline+PC+OB+PNR* are highly concentrated, with fewer retractions.

## 4 Conclusions

In this work, we propose a RL-based IAGN method for robot-assisted EI. This method employs the proposed BDA-star, guiding toward the vascular center, to plan the paths for IAGN, establishing a RL environment comprised of observations that integrate the guidewire tip and planned path, along with a path navigation reward function. Notably, we address the challenge of slow convergence during policy learning by employing a network that combines a pre-trained CNN with a MLP. Experiments on the aortic simulation IAGN platform demonstrated a 100% success rate in guidewire navigation for the LSA and BCA, along with reduced movement and retraction distances, and the trajectories converged towards the central axis of the vessels, revealing its potential in clinical practice.

## References

1. Chi, W., Dagnino, G., Kwok, T.M., Nguyen, A., Kundrat, D., Abdelaziz, M.E., Riga, C., Bicknell, C., Yang, G.Z.: Collaborative robot-assisted endovascular catheterization with generative adversarial imitation learning. In: 2020 IEEE International conference on robotics and automation (ICRA). pp. 2414–2420. IEEE (2020)
2. Chi, W., Liu, J., Abdelaziz, M.E., Dagnino, G., Riga, C., Bicknell, C., Yang, G.Z.: Trajectory optimization of robot-assisted endovascular catheterization with reinforcement learning. In: 2018 IEEE/RSJ International Conference on Intelligent Robots and Systems (IROS). pp. 3875–3881. IEEE (2018)
3. Hart, P.E., Nilsson, N.J., Raphael, B.: A formal basis for the heuristic determination of minimum cost paths. IEEE transactions on Systems Science and Cybernetics 4(2), 100–107 (1968)
4. He, K., Zhang, X., Ren, S., Sun, J.: Deep residual learning for image recognition. In: Proceedings of the IEEE conference on computer vision and pattern recognition. pp. 770–778 (2016)
5. Hwang, J., Kim, J.y., Choi, H.: A review of magnetic actuation systems and magnetically actuated guidewire-and catheter-based microrobots for vascular interventions. Intelligent Service Robotics 13, 1–14 (2020)
6. Jiang, S., Teng, S., Lu, J., Wang, C., Wen, T., Zhu, J., Teng, G.: Pixeltopois: a pixel-topology-coupled guidewire tip segmentation framework for robot-assisted intervention. International Journal of Computer Assisted Radiology and Surgery 17(2), 329–341 (2022)
7. Jianu, T., Huang, B., Abdelaziz, M.E., Vu, M.N., Fichera, S., Lee, C.Y., Berthet-Rayne, P., Nguyen, A., et al.: Cathsim: An open-source simulator for autonomous cannulation. arXiv preprint arXiv:2208.01455 (2022)

8. Jianu, T., Huang, B., Vo, T., Vu, M.N., Kang, J., Nguyen, H., Omisore, O., Berthet-Rayne, P., Fichera, S., Nguyen, A.: Autonomous catheterization with open-source simulator and expert trajectory. arXiv preprint arXiv:2401.09059 (2024)
9. Jocher, G., Chaurasia, A., Qiu, J.: Ultralytics yolov8 (2023), <https://github.com/ultralytics/ultralytics>
10. Kweon, J., Kim, K., Lee, C., Kwon, H., Park, J., Song, K., Kim, Y.I., Park, J., Back, I., Roh, J.H., et al.: Deep reinforcement learning for guidewire navigation in coronary artery phantom. *IEEE Access* **9**, 166409–166422 (2021)
11. Li, H., Zhou, X.H., Xie, X.L., Liu, S.Q., Feng, Z.Q., Hou, Z.G.: Casog: Conservative actor-critic with smooth gradient for skill learning in robot-assisted intervention. arXiv preprint arXiv:2304.09632 (2023)
12. Li, R.Q., Xie, X.L., Zhou, X.H., Liu, S.Q., Ni, Z.L., Zhou, Y.J., Bian, G.B., Hou, Z.G.: Real-time multi-guidewire endpoint localization in fluoroscopy images. *IEEE Transactions on Medical Imaging* **40**(8), 2002–2014 (2021)
13. Liu, W., Tian, T., Wang, L., Xu, W., Li, H., Zhao, W., Pan, X., Yang, H., Gao, F., Deng, Y., et al.: Dias: A comprehensive benchmark for dsa-sequence intracranial artery segmentation. arXiv preprint arXiv:2306.12153 (2023)
14. Liu, W., Yang, H., Tian, T., Cao, Z., Pan, X., Xu, W., Jin, Y., Gao, F.: Full-resolution network and dual-threshold iteration for retinal vessel and coronary angiograph segmentation. *IEEE Journal of Biomedical and Health Informatics* **26**(9), 4623–4634 (2022)
15. Ma, H., Smal, I., Daemen, J., van Walsum, T.: Dynamic coronary roadmapping via catheter tip tracking in x-ray fluoroscopy with deep learning based bayesian filtering. *Medical image analysis* **61**, 101634 (2020)
16. Raffin, A., Hill, A., Gleave, A., Kanervisto, A., Ernestus, M., Dormann, N.: Stable-baselines3: Reliable reinforcement learning implementations. *Journal of Machine Learning Research* **22**(268), 1–8 (2021), <http://jmlr.org/papers/v22/20-1364.html>
17. Su, R., van der Sluijs, M., Chen, Y., Cornelissen, S., van den Broek, R., van Zwam, W., van der Lugt, A., Niessen, W., Ruijters, D., van Walsum, T.: Cave: Cerebral artery-vein segmentation in digital subtraction angiography. arXiv preprint arXiv:2208.02355 (2022)
18. Vaduganathan, M., Mensah, G.A., Turco, J.V., Fuster, V., Roth, G.A.: The global burden of cardiovascular diseases and risk: a compass for future health (2022)
19. Zhao, Y., Guo, S., Wang, Y., Cui, J., Ma, Y., Zeng, Y., Liu, X., Jiang, Y., Li, Y., Shi, L., et al.: A cnn-based prototype method of unstructured surgical state perception and navigation for an endovascular surgery robot. *Medical & Biological Engineering & Computing* **57**, 1875–1887 (2019)
20. Zhou, Y.J., Liu, S.Q., Xie, X.L., Zhou, X.H., Wang, G.A., Hou, Z.G., Li, R.Q., Ni, Z.L., Fan, C.C.: A real-time multi-task framework for guidewire segmentation and endpoint localization in endovascular interventions. In: 2021 IEEE International Conference on Robotics and Automation (ICRA). pp. 13784–13790. IEEE (2021)